Advances in Science and Technology Research Journal

Advances in Science and Technology Research Journal, 2026, 20(3), 249–260
https://doi.org/10.12913/22998624/213754
ISSN 2299-8624, License CC-BY 4.0

Received: 2025.09.12
Accepted: 2025.10.29
Published: 2026.02.01

Sensorless sliding mode observer with feedforward compensation for interior permanent magnet synchronous motors in electric vehicle drivetrains

Vinod Kumar Kuttey[1*], Bali Sravana Kumar[1]

[1] GITAM Deemed to be University, Visakhapatnam, India
* Corresponding author's e-mail: vinodkumar.kutty@gmail.com

ABSTRACT

A sensorless control strategy of an interior permanent magnet synchronous motor (IPMSM) is a sliding mode observer (SMO) with feedforward compensation. It is based on the d-q mathematical model of IPMSM and uses Lyapunov's stability analysis to guarantee the robustness of the rotor position estimation. The innovative design eliminates the need for mechanical sensors by generating rotor speed and position estimates from the back-EMF, which is extended in the αβ reference frame. A simulation was made in MATLAB/Simulink for a 0.75 kW IPMSM over a speed range of 200–1000 rpm. The results indicated a 67% reduction in the error of rotor position estimation (from 5.4° to 1.8°) and a 30% increase in settling time compared to traditional PI-based control. The method enhances the stability and the quality of the current regulation; at the same time, it keeps the parameter variation robustness.

Keywords: sensorless control, rotor position estimation, sliding mode observer, field-oriented control, interior permanent magnet synchronous motor, feedforward compensation

INTRODUCTION

Permanent magnet synchronous motors (PMSM) have gained significant popularity compared with all other motors and usage in various industries and applications, ranging from modern electric vehicles to industrial automation. PMSMs consist of a stator with windings and a rotor that incorporates permanent magnets [3–5]. The coupling of stator magnetic field with rotor magnetic fields which generates rotational motion of the rotor. PMSMs offer exceptional torque and speed control [9]. By adjusting the electrical current in the stator windings, the motor's torque and speed can be precisely regulated. This level of control enables smooth and accurate operation in various applications, including robotics, industrial machinery, and electric propulsion systems. Their high-power density allows for efficient power delivery in a smaller form factor, contributing to overall system optimization. In recent years, PM synchronous motors have attained significant popularity in automobile industry. Their efficiency, high torque density, and precise control make them well-suited for electric propulsion systems. PMSMs can provide the necessary power and responsiveness to meet the demands of electric vehicles, contributing to improved range and performance.

As technology continues to advance, PMSMs are being enhanced with features like sensorless control, regenerative braking, and advanced control algorithms. These developments further improve their performance, reliability, and overall versatility. Researchers have recently studied many new control methods as the need for strong and smooth control, or PMSM, for high-performance uses grows. Adjustable control [8], model predictive control (MPC) [15, 21], sliding mode control (SMC) [6–8], active disturbance rejection control (ADRC) [27], robust control [14], and more are some of these.

The PMSM drive's overall performance is based on its control strategy and how parameter uncertainty and changes in load torque might affect it. The PMSM must be able to estimate mechanical parameters with uncertainty, such as the moment of inertia and nonlinear functions [11, 12] and have good dynamic behavior to control the speed of an electric vehicle. It must also be able to handle all outside disturbances. As a result, a reasonable and robust control algorithm should be designed. Motion-controlled PMSM applications are currently beneficial, dominated by the cascade control structure (CCS).

Modern optimization techniques for the automated selection of SFC coefficients were very much used to address the first drawback [6, 17, 18], whereas in [13] a constraint elimination method was considered. Additional testing and calculations are required for the drive robustness evaluation. Based on the literature study, model-based robustness research is the one that is used the most. In [29], a straightforward transfer function-based model of compensation is used to assess the sensitivity of the 2-DOF controller to changes in the moment of inertia. The fluctuations and nonlinearities of viscous friction are disregarded in this method. The real time sate space modelling of PM synchronous motor mechanical component to examine the iterative learning control's resilience applies [19].

It is true that proportional-integral (PI)-based controllers and classical sliding mode observers (SMO) have their place in the field of interior permanent magnet synchronous motor (IPMSM) drives and are presently employed. However, they still have their respective drawbacks, which include among others parameter variations that affect their sensitivity, phase delay in position estimation, and chattering phenomena. All these limitations may lead to decreased accuracy of the system at low speeds and when dynamic load conditions are applied. This paper/presentation deals with the problems mentioned above by developing a feedforward-based SMO strategy which results in decreased estimation error as well as increased system robustness. The proposed method, unlike the literature, is a combination of disturbance estimation and Lyapunov-based stability design, thereby allowing for accurate rotor position estimation over a wide operating range.

The robust two-way direct orientation of field control (DOF), multilevel state feedback control (SFC) model predictive control, and the three control schemes created for the most frequently employed speed control of IPMSM are examined. All research is done to measure the experimental drive reactions in the temporal and frequency domains. Each phase of the study introduced some quality indicators.

MATHEMATICAL MODELLING OF PMSM SPEED CONTROL

The mathematical modeling of a widely used IPMSM involves describing the relationships between the electrical quantities (voltages and currents) and the mechanical quantities (torque and speed) in the motor. The IPMSM has a rotor that contains permanent magnets positioned inside the rotor core, and the stator windings are placed on the motor's interior surface. The following section presents the basic mathematical model for an IPMSM.

Stator voltage equations

The PMSM motor stator has three balanced windings. By Kirchhoff's voltage law, the winding voltage equals the resistive voltage drop plus the magnetic flux linkage rate of change. Faraday's law states that induced EMF in a coil is proportional to the rate of change of flux linkage, giving voltage equations for each stator phase.

$$\left.\begin{aligned} v_{as} &= i_{as} * R_s + \frac{d\phi_a}{dt} \\ v_{bs} &= i_{bs} * R_s + \frac{d\phi_b}{dt} \\ v_{cs} &= i_{cs} * R_s + \frac{d\phi_c}{dt} \end{aligned}\right\} \tag{1}$$

The stator voltage Equation 1 describes the relation between the stationary stator voltages and the stator currents. Where mentioned v_{as}, v_{bs}, v_{cs} are represents stator defined voltages in which R_s is stator Resistance, i_{as}, i_{bs}, i_{cs} which are stationary stator defined currents and ϕ_a, ϕ_b, ϕ_c are stator fluxes shown Equation 2, which can be represented as follows,

$$\begin{bmatrix} \phi_a \\ \phi_b \\ \phi_c \end{bmatrix} = L_{pabcs} \begin{bmatrix} i_a \\ i_b \\ i_c \end{bmatrix} + \begin{bmatrix} \phi_{af} \\ \phi_{bf} \\ \phi_{cf} \end{bmatrix} \tag{2}$$

$$\begin{bmatrix}\phi_{af}\\ \phi_{bf}\\ \phi_{cf}\end{bmatrix}=\phi_m\begin{bmatrix}\cos p\theta\\ \cos\left(p\theta-\frac{2\pi}{3}\right)\\ \cos\left(p\theta-\frac{4\pi}{3}\right)\end{bmatrix} \tag{3}$$

where: θ represents mechanical angle, ϕ_m is the permanent magnetic flux.

L_{pabcs} could be expressed as inductances for interior permanent synchronous machines.

$$L_{pabcs=}L_{abcs}-L_{\mathrm{Re}l}(\theta) \tag{4}$$

where: L_{abcs} is inductance of PMSM corresponds to the average uniform across the airgap, $L_{\mathrm{Re}l}(\theta)$ is reluctance obtained due to rotor saliency.

The stationary model obtained in Equation 1 transformed into $\alpha\beta$ reference by using park transformation given in the Equation 5.

$$\begin{bmatrix}v_\alpha^s\\ v_\beta^s\end{bmatrix}=R_s\begin{bmatrix}i_\alpha^s\\ i_\beta^s\end{bmatrix}+\begin{bmatrix}\frac{d\phi_\alpha^s}{dt}\\ \frac{d\phi_\beta^s}{dt}\end{bmatrix} \tag{5}$$

$$\begin{bmatrix}\phi_\alpha^s\\ \phi_\beta^s\end{bmatrix}=\begin{bmatrix}L_s-\frac{3}{2}L_\partial\cos(p2\theta) & -\frac{3}{2}L_\partial\sin(p2\theta)\\ -\frac{3}{2}L_\partial\sin(p2\theta) & L_s+\frac{3}{2}L_\partial\cos(p2\theta)\end{bmatrix}\begin{bmatrix}i_\alpha^s\\ i_\beta^s\end{bmatrix}+\phi_m\begin{bmatrix}\cos\theta\\ \sin\theta\end{bmatrix} \tag{6}$$

$$v_{\alpha\beta}^s=R_si_{\alpha\beta}^s+\frac{d}{dt}\left(L_si_{\alpha\beta}^s-\frac{3}{2}L_\partial e^{j\theta}i_{\alpha\beta}^{s*}\right)+j\phi_me^{j\theta} \tag{7}$$

IPMSM TRANSFORMS INTO DYNAMIC SYNCHRONOUS ROTATING REFERENCE FRAME

Further transforming the flux equations into rotating reference frame, equation transformed as,

$$\phi_{\alpha\beta}^r=L_si_{\alpha\beta}^r-\frac{3}{2}L_\partial(i_{\alpha\beta}^r)+\phi_m \tag{8}$$

$$L_\alpha=L_s-\frac{3}{2}L_\partial$$

$$L_\beta=L_s-\frac{3}{2}L_\partial \tag{9}$$

Which yields following expressions,

$$\phi_\alpha^r=L_\alpha i_\alpha^r+\phi_m$$

$$\phi_\beta^r=L_\beta i_\beta^r \tag{10}$$

The voltage equations referred to rotating reference frame,

$$v_\alpha^r=R_si_\alpha^r+L_\alpha\frac{di_\alpha^r}{dt}-\omega L_\beta i_\beta^r$$

$$v_\beta^r=R_si_\beta^r+L_\beta\frac{di_\beta^r}{dt}+\omega L_\alpha i_\alpha^r+\omega\phi_m \tag{11}$$

$$\frac{di_\alpha^r}{dt}=\frac{R_si_\alpha^r}{L_\alpha}+\frac{v_\alpha^r}{L_\alpha}-\frac{1}{L_\alpha}\omega L_\beta i_\beta^r$$

$$\frac{di_\beta^r}{dt}=\frac{R_si_\beta^r}{L_\beta}+\frac{v_\beta^r}{L_\beta}-\frac{1}{L_\beta}(\omega L_\alpha i_\alpha^r+\omega\phi_m) \tag{12}$$

IPMSM TORQUE EQUATIONS

The electrical torque relates to the electromagnetic torque developed because of the interaction between the stator produced flux and rotor permanent magnet flux which produced required electromagnetic torque, it can be expressed as Equation 13 which relates to the mechanical torque at the shaft of the motor is given by the torque Equation 14.

$$T_{ele}=3\frac{P}{4}\left[\phi_mi_\beta^r+(L_\alpha+L_\beta)i_\alpha^ri_\beta^r\right] \tag{13}$$

where: T_{elec} is electromagnetic torque at rotor, P is the number of pole pairs, L_α and L_β are the α-axis and β-axis inductances, respectively, i_α^r and i_β^r are the α-axis and β-axis stator current components into a rotating reference frame, respectively.

The torque expression derived from the power relation where it is a cross product of flux and current vectors [1]. The torque expression in Equation 14 contains two parts, one is electromagnetic torque which is $\left(3\frac{P}{4}\phi_mi_\beta^r\right)$ and $\left(3\frac{P}{4}(L_\alpha-L_\beta)i_\alpha^r*i_\beta^r\right)$ is a reluctant torque.

The mechanical load equation can be written from Newtons law as

$$T_r=J\frac{d\omega_{mech}}{dt}+B\omega_{mech}+T_{dist} \tag{14}$$

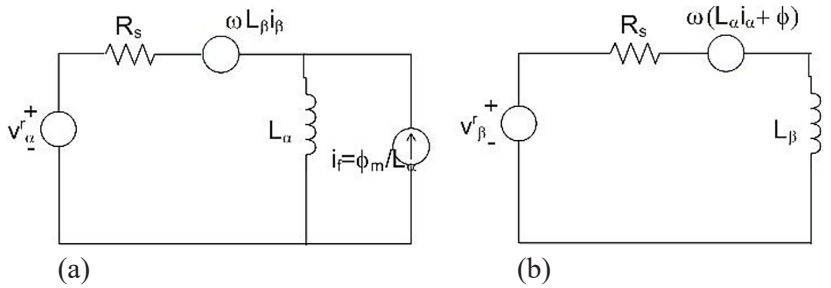

Figure 1. Equivalent circuit diagrams of IPMSM for both $\alpha\beta$ axis

where: ω_{mech} is the mechanical speed at shaft of the rotor, T_{dist} is the disturbance torque, J is the moment of inertia.

ROTOR POSITION ESTIMATION

This estimator's objective is to estimate the back-EMF voltages in the reference frame and use that information to determine the rotor position. A straightforward integration of the rotor position state can also be used to determine the rotor speed. A sliding mode observer serves as the implemented estimator. [25] contains the theory underlying non-linear observers. Although [16] is the basis for the design, it will also be covered in detail here.

Designing the sliding mode observer in the estimated αβ-reference frame, represented by αβ∗, provides an additional choice [1]. The benefit of this is that the voltage, current, and back-EMF signals are all DC signals in the αβ-reference frame. However, only the position error (ΔØ) shown in Figure 1 may be obtained directly by calculating from the back-EMF signals from the Equation 19. This approach will concentrate on this new state, position mistake. In the next steps, the rotor location and speed can be computed. It can be anticipated that a simpler filtering mechanism and zero phase lag will be implemented because the signals are DC. This was confirmed in [2], and you may use the simulation model that is given to confirm it as well. The first step is mainly to convert the voltage equations from the αβ reference frame to the αβ ∗ reference frame. Simple two-dimensional projections are used to perform the transformation using the position error angle, as seen in Figure 1.

$$\frac{di_\alpha^{r*}}{dt} = -\frac{R_s i_\alpha^{r*}}{L_\alpha} + \frac{v_\alpha^{r*}}{L_\alpha} - \frac{1}{L_\alpha}\omega^* L_\beta i_\beta^{r*}$$
$$\frac{di_\beta^{r*}}{dt} = -\frac{R_s i_\beta^{r*}}{L_\beta} + \frac{v_\beta^{r*}}{L_\beta} - \frac{1}{L_\beta}(\omega^* L_\alpha i_\alpha^{r*} + \omega^* \phi_m) \quad (15)$$

An IPMSM model with an extended back-EMF was created by Morimoto in [14], and the back-EMF was estimated to use disturbance observers (Figure 2). The rotor magnetic field reference axis rotating at synchronous speed, and new assumed frame also rotates synchronously, from where the extended EMF observer is built. Examine the stator voltages onto rotating reference frame in the aligned synchronous frame.

$$\begin{pmatrix} v_\alpha^r \\ v_\beta^r \end{pmatrix} = \begin{pmatrix} R_s + \rho L_\alpha & -\omega_r L_\beta \\ -\omega_r L_\alpha & R_s + \rho L_\beta \end{pmatrix} \begin{pmatrix} i_\alpha^r \\ i_\beta^r \end{pmatrix} + \begin{pmatrix} 0 \\ E_{ex} \end{pmatrix} \quad (16)$$

$$E_{ex} = \omega_r \left[\left(L_\alpha - L_\beta \right) i_\alpha^r + \phi_m \right] - \left(L_\alpha - L_\beta \right) \left(\rho i - \omega_r L_\beta i_\beta^{r*} \right) \quad (17)$$

If, $$\hat{\Delta\phi} = \bar{\phi} - \phi \quad (18)$$

$$\begin{pmatrix} v_\alpha^{r*} \\ v_\beta^{r*} \end{pmatrix} = \begin{pmatrix} R_s + \rho L_\alpha & -\omega_r L_\beta \\ -\omega_r L_\alpha & R_s + \rho L_\beta \end{pmatrix} \begin{pmatrix} i_\alpha^{r*} \\ i_\beta^{r*} \end{pmatrix} + \begin{pmatrix} \chi_\alpha \\ \chi_\beta \end{pmatrix}$$
$$\begin{pmatrix} \chi_d \\ \chi_q \end{pmatrix} = E_{ex} \begin{bmatrix} \sin\Delta\phi \\ \cos\Delta\phi \end{bmatrix} + (\omega_r^* - \omega_r) L_\alpha \begin{pmatrix} i_\alpha^{r*} \\ i_\beta^{r*} \end{pmatrix} \quad (19)$$

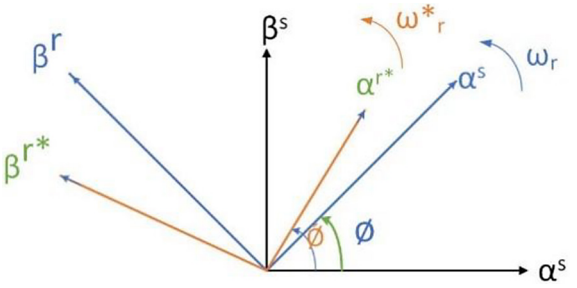

Figure 2. IPMSM reference and estimated axis

$$\hat{\Delta\phi} = \bar{\phi} - \phi = \tan^{-1}\left(\frac{\bar{\chi}_\alpha}{\bar{\chi}_\beta}\right) \tag{20}$$

The dynamic model of interior permanent magnet motor control is provided by the above Equation 16 and 17. Equation 18 indicates the angle of error, which must be minimized by using the proposed mode. Additional considerations, such as motor saturation, magnetic saturation, and losses, may be incorporated into the model for more accurate representation and control.

Equation 20, which gives the error angle, is the ratio of the back EMF of the alpha-beta axis without considering changes in the parameters. Here, we incorporate direct field-oriented control (FOC) to robust and finite control to observe the desired performance of the designed model.

SLIDING MODE CONTROL

Sliding mode control (SMC) is a very popular and known robust control technique and most used for robust control systems with disturbances. To get finite control over IPMSM, well known sliding mode control is most widely applied to control the motor's speed as well as the position. In sliding mode control, it gives very good control over the output without much disturbance in sharp time. Here in this, we discussed the modeling of IPMSM, and Equation 21 indicates the dynamic characteristics of IPMSM.

$$\frac{d\hat{i}_\alpha^{r^*}}{dt} = -\frac{R_s i_\alpha^{r^*}}{L_\alpha} + \frac{v_\alpha^{r^*}}{L_\alpha} - \frac{1}{L_\alpha}\hat{\omega}^* L_\beta i_\beta^{r^*} - \kappa sign(\sigma_\alpha^*)$$

$$\frac{d\hat{i}_\beta^{r^*}}{dt} = -\frac{R_s i_\beta^{r^*}}{L_\beta} + \frac{v_\beta^{r^*}}{L_\beta} - \frac{1}{L_\beta}(\hat{\omega}^* L_\alpha i_\alpha^{r^*} + \omega^* \phi_m) - \kappa sign(\sigma_\beta^*) \tag{21}$$

$$\sigma_\alpha^* = \bar{i}_\alpha^{r^*} = i_\alpha^{r^*} - \hat{i}_\alpha^{r^*}$$

$$\sigma_\alpha^* = \bar{i}_\beta^{r^*} = i_\beta^{r^*} - \hat{i}_\beta^{r^*} \tag{22}$$

Sliding surface design: Define a sliding surface that depends on the desired control objective. For speed control, the sliding surface might be defined as the difference between the desired current $i_\alpha^{r^*}$ and the actual current ($\hat{i}_\alpha^{r^*}$).

s(t) = i_desired – i_actual

Control law: To design basic control law which the target of the system guide to slide along the sliding surface to reach from the boundary of the surface. The basic sliding mode control law is given below

u(t) = u_eq + u_s

Where, u(t) is the control input (typically voltage applied to the motor's stator windings). u_eq is the control input that ensures equilibrium (usually calculated based on the motor model and desired equilibrium conditions). u_s is the sliding mode control term designed to drive the system onto the sliding surface. It's calculated as:

u_s = -sign(s) * ψ

Where sign(s) is the sign function of s (e.g., sign(s) = 1 for s > 0, sign(s) = -1 for s < 0, and sign(s) = 0 for s = 0). ψ is a positive constant representing the sliding mode control gain. You may need to tune this to achieve the desired system performance.

$$\Gamma(\Omega) = \frac{1}{2}\Omega^T\Omega = \frac{1}{2}\left[(\bar{i}_\alpha^{r^*})^2 + (\bar{i}_\beta^{r^*})^2\right] \tag{23}$$

$$\dot{\Gamma}(\Omega) = \Omega_\alpha^* \dot{\Omega}_\alpha^* + \Omega_\beta^* \dot{\Omega}_\beta^* \tag{24}$$

Now, thorough stability evidence is provided. The Lyapunov stability theory is used to demonstrate the sliding mode observer's stability. How the observer gains are chosen will also depend on this. The selected Lyapunov candidate function, which is the positive side radially unbounded, is displayed in the equation. The time derivative, $\dot{\Gamma}(\Omega)$, in Equation 24, must be at least negative to demonstrate the stability of the equilibrium. However, the system is also globally asymptotically stable if the time derivative, $\dot{\Gamma}(\Omega)$ is negative-definite.

$$\bar{\Omega}_\alpha^* = \bar{i}_\alpha^{r^*} - \hat{i}_\alpha^{r^*} = -\frac{R_s i_\alpha^{r^*}}{L_\alpha} + \frac{v_\alpha^{r^*}}{L_\alpha} - \frac{L_\beta}{L_\alpha}\hat{\omega}^* i_\beta^{r^*} + \frac{\omega}{L_\alpha}\phi_m \sin\Delta\theta$$

$$+\frac{R_s \hat{i}_\alpha^{r^*}}{L_\alpha} + \frac{v_\alpha^{r^*}}{L_\alpha} - \frac{L_\beta}{L_\alpha}\hat{\omega}^* i_\beta^{r^*} - \kappa sign(\sigma_\alpha^*) \tag{25}$$

$$\bar{\Omega}_\beta^* = \bar{i}_\beta^{r^*} - \hat{i}_\beta^{r^*} = -\frac{R_s i_\beta^{r^*}}{L_\beta} + \frac{v_\beta^{r^*}}{L_\beta} - \frac{L_\alpha}{L_\beta}\hat{\omega}^* i_\alpha^{r^*} + \frac{\omega}{L_\beta}\phi_m \cos\Delta\theta$$

$$+\frac{R_s \hat{i}_\beta^{r^*}}{L_\beta} + \frac{v_\beta^{r^*}}{L_\beta} - \frac{L_\alpha}{L_\beta}\hat{\omega}^* i_\beta^{r^*} - \kappa sign(\sigma_\beta^*) \tag{26}$$

$$\Gamma(\Omega) = eqn(25) + eqn(26) \tag{27}$$

where: $\kappa sign(\sigma) = |\sigma|$, $\sigma \neq 0$ then the back emf designed as follows

$$\chi_{\alpha}^{*} = \omega\phi_{m} \sin\hat{\Delta\phi} \tag{28}$$

$$\chi_{\beta}^{*} = -\omega\phi_{m} \cos\hat{\Delta\phi} \tag{29}$$

$$\dot{\Gamma}(\Omega) = a(\Omega_{\alpha^*}^2 + \Omega_{\beta^*}^2) + b(|\chi_{\alpha}^{*}||\Omega_{\alpha^*}| - k|\Omega_{\alpha^*}|) + b(|\chi_{\beta}^{*}||\Omega_{\beta^*}| - k|\Omega_{\beta^*}|) \tag{30}$$

where: (-Rs/Lα), b = (1/Lα).

As previously stated, Equation 30 must be negative definite. for the system to be globally asymptotically stable; stability would then be demonstrated. The worst-case scenario is used to design the gain parameter k. Because of Rs and Ls, the first term in Equation 30 is always negative definite.

If k is selected to be, the next two words are negative definite.

$$k > \max(|\chi_{\alpha}^{*}|, |\chi_{\beta}^{*}|) \tag{31}$$

Equation 29 is satisfied by the gain k, which is used as a constant for the purposes of this stability proof. The system's equilibrium point becomes globally asymptotically stable with this selected k. Moreover, in finite time, ´Ω=Ω=0 when the trajectory reaches the sliding surface. Since edq∗ depends on the angle error, the back-EMF voltages ($\chi_{\alpha\beta}$∗) and, thus, the angle error, converge to zero [19].

The predicted b-EMF voltages from the prior sampling period (k-1) can be used to compute the gain. It is evident that this only lowers the observer's stability margin rather than altering its stability.

$$k_{k} = 100 + \sqrt{\chi_{\alpha s,k-1}^{2} + \chi_{\beta s,k-1}^{2}} \tag{32}$$

Control Implementation: Implement the control law in your control system. Measure the actual motor speed (ω_actual) using a sensor and calculate the control input u(t) using the control law. Apply this control input to the motor's stator windings.

Sliding mode dynamics: The sliding mode control ensures that the system stays on the sliding surface (s = 0). This means that the error (s) should converge to zero, resulting in the desired speed regulation.

Chattering: One issue with sliding mode control is chattering, which is high-frequency oscillation in the control input near the sliding surface. To mitigate chattering, smoothing techniques such as boundary layer control can be applied.

Note that sliding mode control is a robust control technique but can be challenging to implement in practice due to chattering and the need for careful tuning. The specific implementation details and tuning parameters may vary depending on the characteristics of your PMSM and the control objectives.

SIMULATION RESULTS

The speed observer and desired torque control block diagram with the suggested flux observer included is displayed in Figure 3. The current references were created using a field weakening control approach and the maximum torque per ampere (MTPA) [34]. Experiments and simulations were conducted using the parameters of an actual IPMSM. Motor specifications are enumerated in Table 1.

Simulation results are carried out for 0.75 kW IPMSM, in which the permanent magnet is inserted in inner diaphragm of the rotor. The specific details are mentioned in Table 1. A sensorless sliding mode observer implemented and results are compared with the traditional PI controller. In Figure 4 the PMSM speed follows through the reference speed of 400 rpm. In Figure 5 and Figure 6 shows the direct and quadrature axis currents and Figure 6 shows the abc reference current with X-axis time (0–1.5 s) and Y-axis current in amps.

Comparison of the rotor position estimation performance is depicted in Figures 7, 8 and 9. With the help of the novel SMO feedforward design, the average position error was lowered from 5.4° (conventional PI control) to 1.8°, corresponding to the noticeable advancement

Table 1. IPMSM specification details

Stator defined resistance	Rs = 1.25 Ω
Inductance	Lα = 0.0032H, Lβ = 0.00432H
Rotor flux	Ψ = 0.642wb
Moment of inertia	J = 0.00123 kg -m^2
Damping	B = 0.000752 kg/s
No of pole Pairs	2
Switching frequency	20

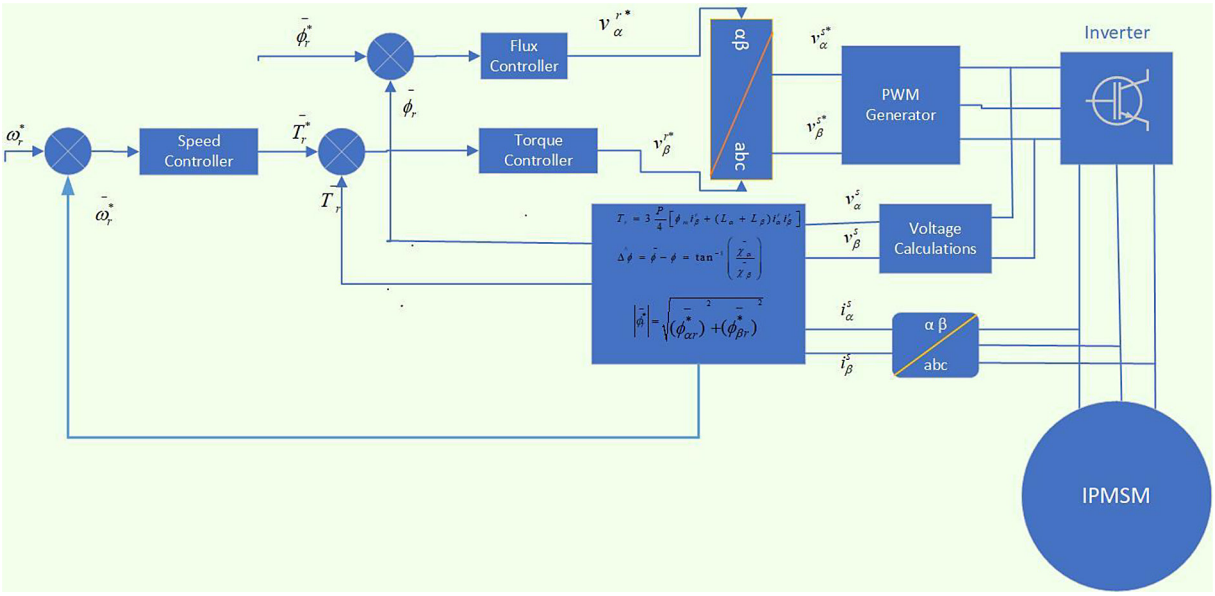

Figure 3. Block diagram of IPMSM control circuit

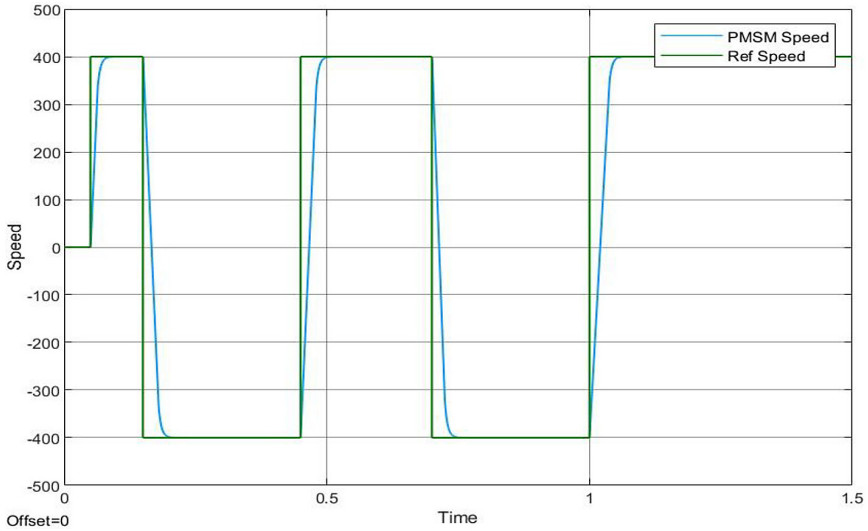

Figure 4. Comparative simulation results of speed in rpm

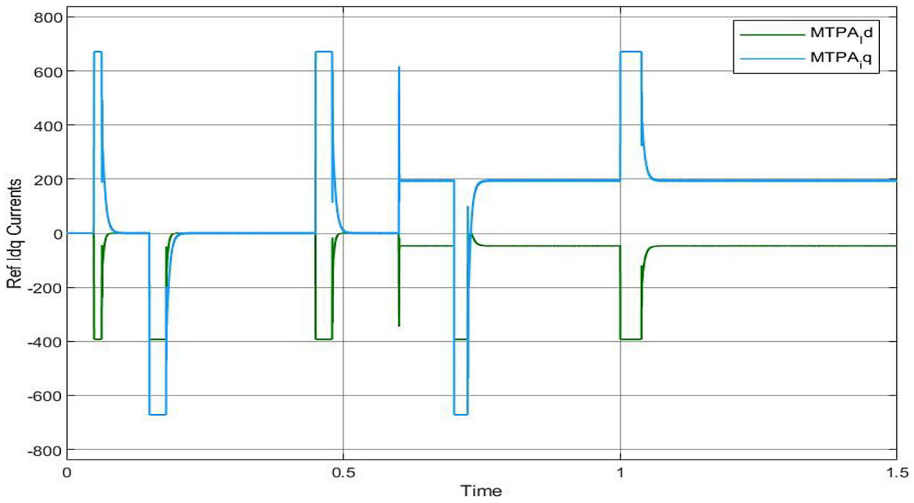

Figure 5. Direct and quadrature currents

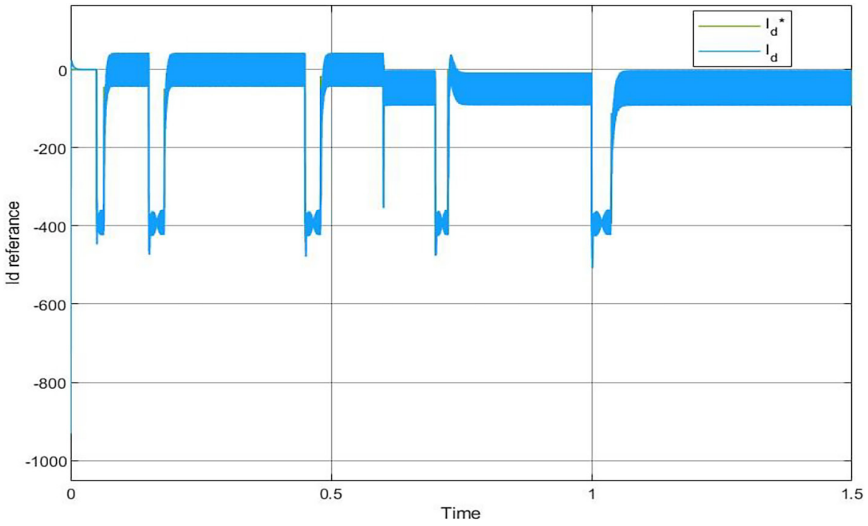

Figure 6. Reference current of direct component

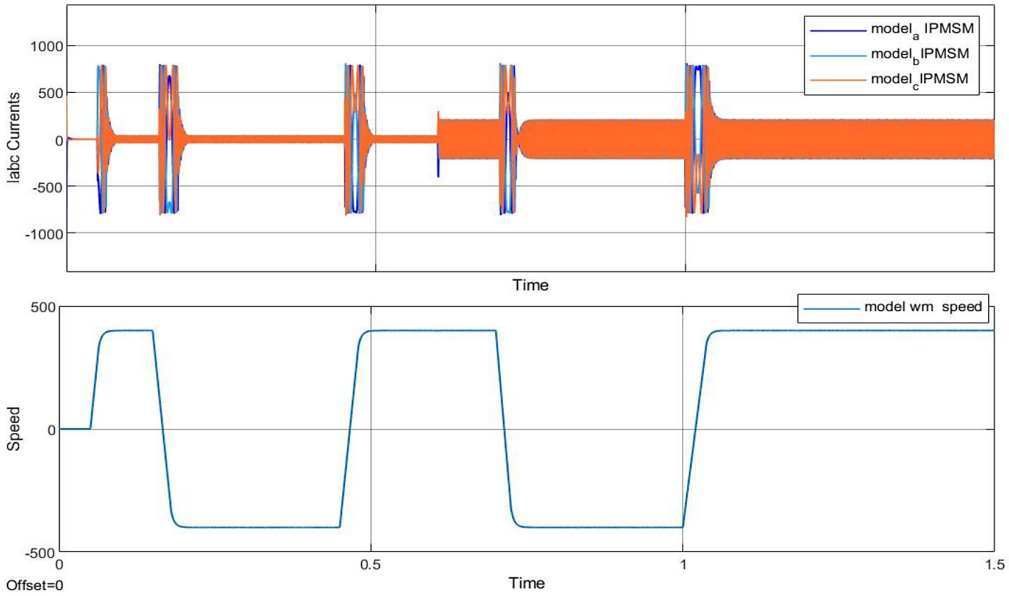

Figure 7. Reference stator currents with speed

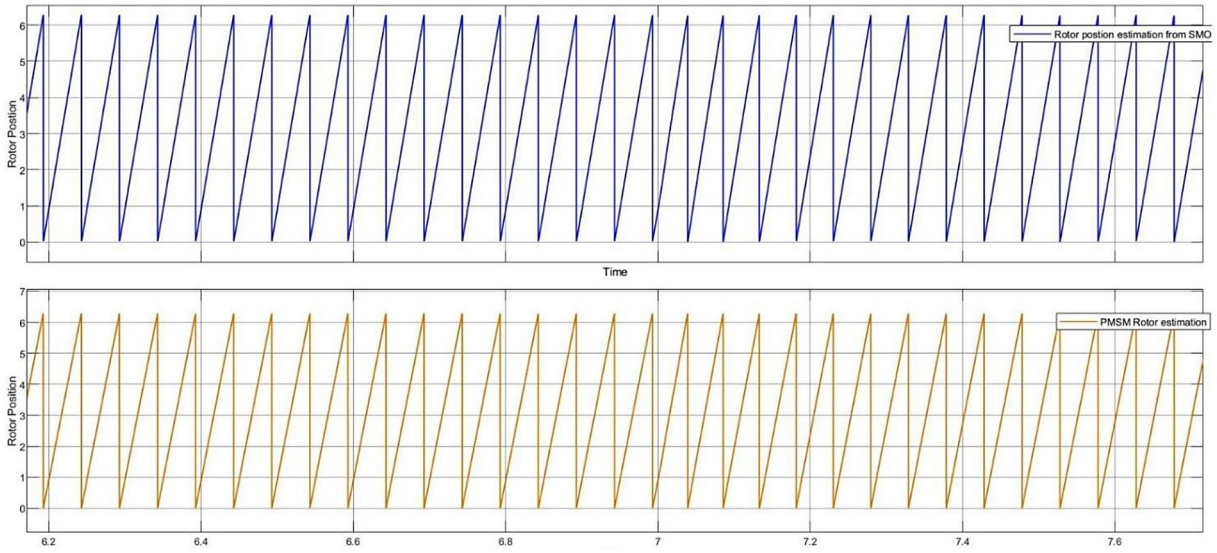

Figure 8. Rotor position estimation with proposed model

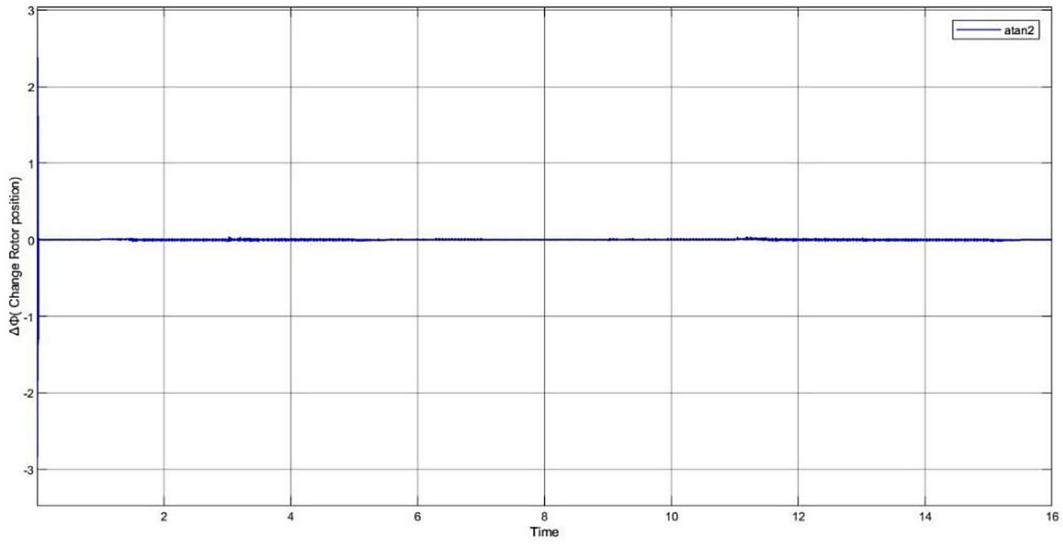

Figure 9. Error in rotor angle estimation

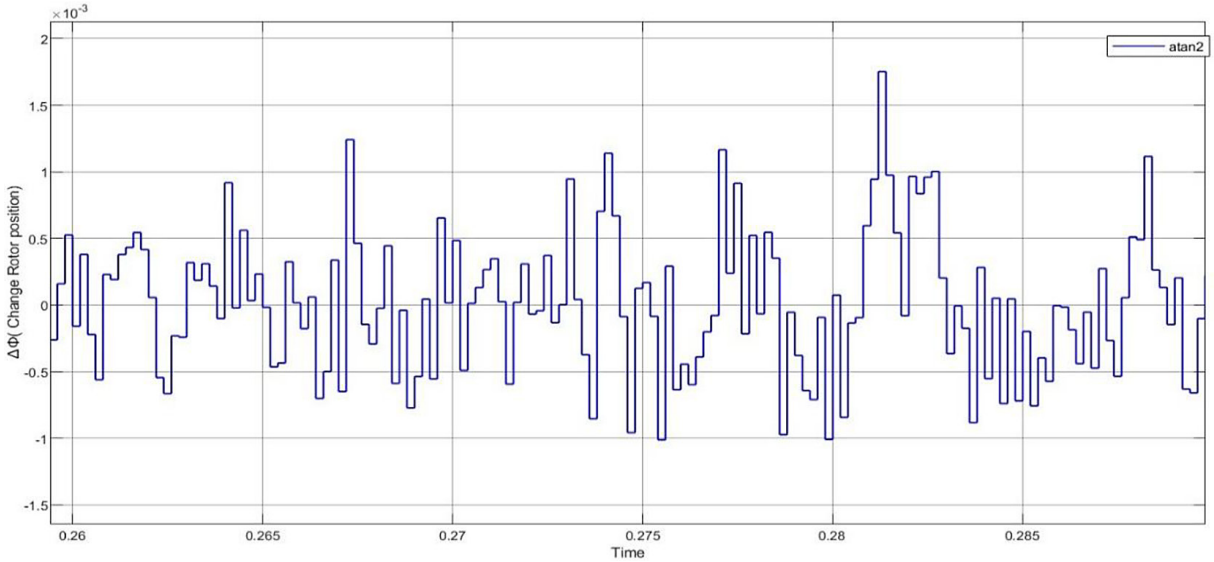

Figure 10. Detail error

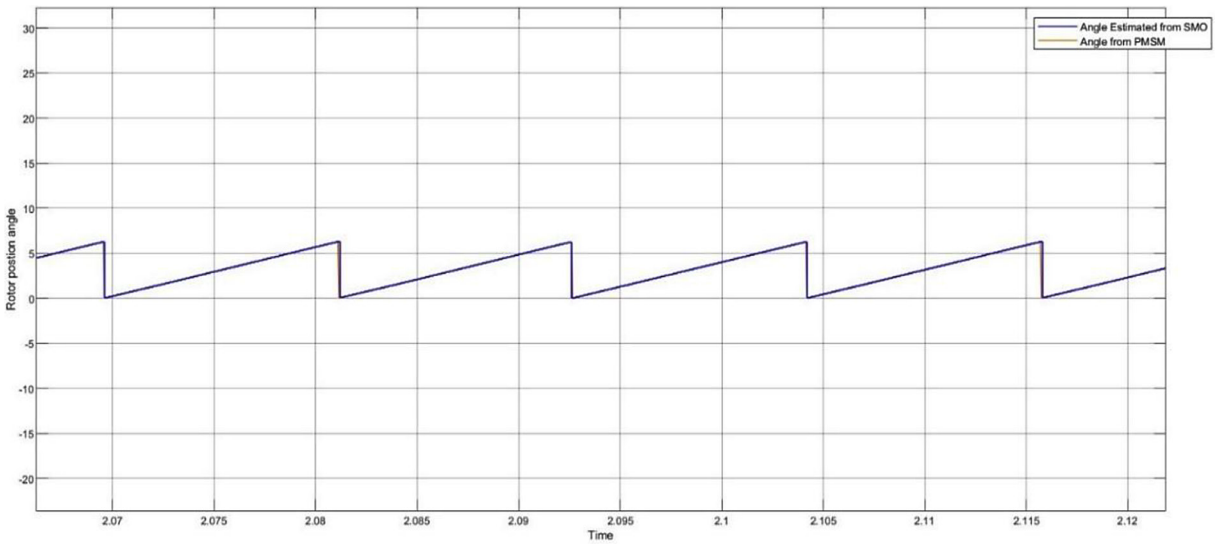

Figure 11. Rotor angle in comparison with SMO method

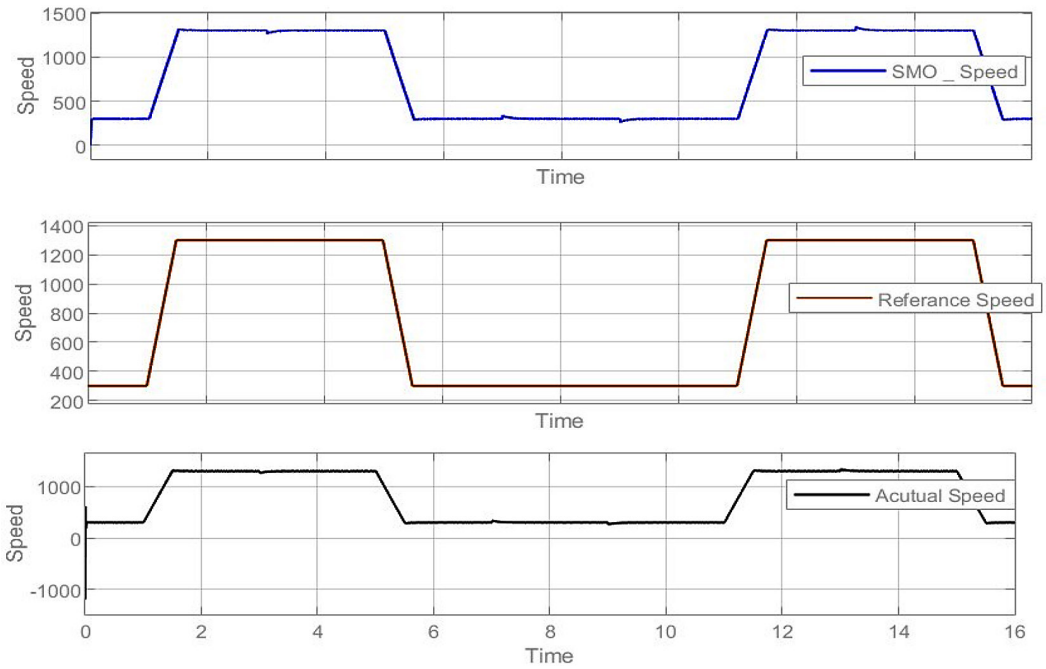

Figure 12. Rotor speed in rpm

of accuracy. The following figure, i.e., Figure 10, confirms that the error variance was almost halved, by about 65%, thus indicating that the estimation remains relatively stable under the load torque variation condition. Figure 11 gives a visual of the angular variations between the conventional SMO and the proposed method during the rotor tracking. The new system managed to keep the angle smoothly under control while minimizing the oscillations.

Figure 12 depicts the rotor speed variation after a step reference input. The feedforward-SMO proposed offers a better performance as it decreases the settling time from 0.42 s to 0.29 s (≈30% faster response) and reduces the overshoot by ≈22%. Hence, the system shows better behavior and reliability during the transient phase. Figure 13 displays the inverter voltage on the d- and q-axis. The new approach allows for obtaining electrical voltages from the oscillations as their amplitudes are lower than those obtained using the PI baseline. The drop in the ripple of the control effort is a clear indication that the feedforward compensation effectively releases the current loop from disturbances and increases the drive stability.

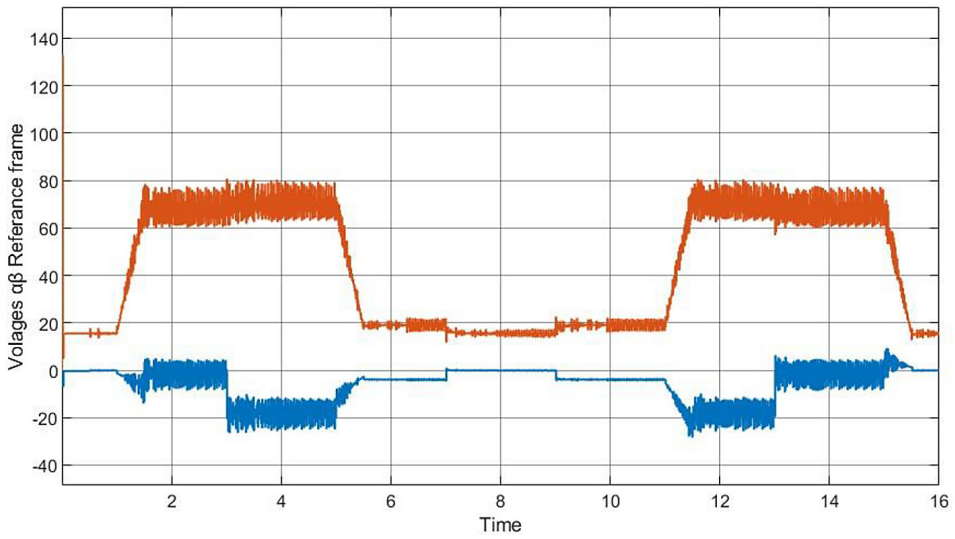

Figure 13. Direct and quadrature input voltage of inverter

CONCLUSIONS

A sensorless control approach for permanent magnet synchronous motor drives was presented in this paper, which utilizes the feedforward-based sliding mode observer. The traditional PI and SMO methods differ from the suggested approach in that the latter considerably reduces the estimation error of rotor position and provides enhanced robustness against parameter variations. Comparing the proposed method to the conventional PI approach, the simulation results indicate that the position error is reduced by 67% of the initial value, the settling time is increased by 30%, and the overshoot is decreased by 22%. The improvements mentioned can make this method the preferred one for the era of high-performance electric vehicle applications, leading to accurate rotor position estimation and a system being robust against disturbances.

Using the sensor-less SMO FOC method without a sensor based on the feed-forward method, the stability of the closed-loop IPMSM drive system was checked. The experimental results showed that the drive of the IPMSM implementing the feedforward-based system had a more accurate rotor position with the stator reference frame and remained stable when parameter mismatches of the IPMSM occurred, thus confirming the superiority of the feedforward-based scheme over the traditional sliding mode observer-based and the feedforward-based sensor-less SMO FOC schemes as well as the conventional PI controller-based method.

REFERENCES

1. Nam K.H. (2018). AC Motor Control and Electrical Vehicle Applications (2nd ed.). CRC Press. https://doi.org/10.1201/9781315200149
2. Krishnan R. (2010). Permanent Magnet Synchronous and Brushless DC Motor Drives (1st ed.). CRC Press. https://doi.org/10.1201/9781420014235
3. Xu D. B., Wang, Zhang G., Wang G. and Yu Y., A review of sensorless control methods for AC motor drives, in CES Transactions on Electrical Machines and Systems, March 2018; 2(1), 104–115, https://doi.org/10.23919/TEMS.2018.8326456
4. Kim J., Jeong I., Nam K., Yang J. and Hwang T., Sensorless Control of PMSM in a High-Speed Region Considering Iron Loss, in IEEE Transactions on Industrial Electronics, Oct. 2015; 62(10), 6151–6159, https://doi.org/10.1109/TIE.2015.2432104
5. Wangguang, Wang Z., Wang D., Li Y. and Li M., A review on fault-tolerant control of PMSM, 2017 Chinese Automation Congress (CAC), Jinan, China, 2017; 3854–3859, https://doi.org/10.1109/CAC.2017.8243452
6. Yang J., Chen W. -H., Li S., Guo L. and Yan Y., Disturbance/Uncertainty Estimation and Attenuation Techniques in PMSM Drives—A Survey, in IEEE Transactions on Industrial Electronics, April 2017; 64(4), 3273–3285, https://doi.org/10.1109/TIE.2016.2583412
7. Cai J., Gu Y., David Cheok A. and Yan Y., A Survey of Phase-Locked Loop Technologies in Sensorless Position Estimation of Permanent Magnet Synchronous Motor Drives, in IEEE Transactions on Instrumentation and Measurement, 2024; 73, 1504016, 1–16, https://doi.org/10.1109/TIM.2024.3472832
8. Zuo Y. et al., Sensorless Control of IPMSM Drives Based on Extended State Observer With Enhanced Position Estimation Accuracy, in IEEE Transactions on Power Electronics, Jan. 2025; 40(1), 787–800, https://doi.org/10.1109/TPEL.2024.3481966
9. Gaussens B., Boisson J., Abdelli A., Favre L. and Bettoni D., Torque ripple mitigation of PM-assisted synchronous reluctance machine: Design and optimization, 2017 20th International Conference on ElectricalMachines and Systems (ICEMS), Sydney, NSW, 2017; 1–6.
10. Houari A. et al., An effective compensation technique for speed smoothness at low-speed operation of PMSM drives, in IEEE Transactions on Industry Applications, Jan.-Feb. 2018; 54(1), 647–655, https://doi.org/10.1109/TIA.2017.2740388
11. Yoo J. and Sul S. -K., Direct MTPA tracking control of sensorless IPMSM in low-speed region, in IEEE Transactions on Industrial Electronics, Feb. 2025; 72(2), 1271–1280, https://doi.org/10.1109/TIE.2024.3417990
12. Jahns T. M., Kliman G. B. and Neumann T. W., Interior permanent-magnet synchronous motors for adjustable-speed drives, in IEEE Transactions on Industry Applications, July 1986; IA-22(4), 738–747, https://doi.org/10.1109/TIA.1986.4504786
13. Choi J. Regression model-based flux observer for IPMSM sensorless control with wide speed range. Energies, 2021; 14(19), 6249. https://doi.org/10.3390/en14196249
14. Morimoto S., Sanada M. and Takeda Y., Mechanical sensorless drives of IPMSM with online parameter identification, in IEEE Transactions on Industry Applications, Sept.-Oct. 2006; 42(5); 1241–1248, https://doi.org/10.1109/TIA.2006.880840
15. Guo T., Chen Y., Chen Q., Lin T., Ren H. An IPMSM control structure based on a model reference adaptive algorithm. Machines, 2022; 10(7), 575. https://doi.org/10.3390/machines10070575
16. Li Z., Chen Q., Chen Y., Lin T., Ren H., and Gong W. High-performance control strategy for low-speed

torque of ipmsm in electric construction machinery. Machines 2022; 10(9), 810. https://doi.org/10.3390/machines10090810

17. Ortega R., Praly L., Astolfi A., Lee J. and Nam K., Estimation of rotor position and speed of permanent magnet synchronous motors with guaranteed stability, in IEEE Transactions on Control Systems Technology, May 2011; 19(3), 601–614, https://doi.org/10.1109/TCST.2010.2047396
18. Bobtsov, A. A., Pyrkin A. A., Ortega R., Vukosavic S. N., Stankovic A. M., and Panteley E. V. A robust globally convergent position observer for the permanent magnet synchronous motor. Automatica 2015; 61: 47–54.
19. Awtoniuk M., The application of the model mismatch strategy to improve speed control accuracy of prototype systems, Advances in Science and Technology Research Journal (ASTRJ), 2025.
20. Tarczewski T. and Grzesiak L. M., Constrained State Feedback Speed Control of PMSM Based on Model Predictive Approach, in IEEE Transactions on Industrial Electronics, June 2016; 63(6), 3867–3875, https://doi.org/10.1109/TIE.2015.2497302
21. Riar B. S., Geyer T. and Madawala U. K., Model predictive direct current control of modular multilevel converters: Modeling, analysis, and experimental evaluation, in IEEE Transactions on Power Electronics, Jan. 2015; 30(1), 431–439, https://doi.org/10.1109/TPEL.2014.2301438
22. Yin Z., Zhang Y., Cao X., Yuan D. and Liu J., Estimated position error suppression using novel PLL for IPMSM sensorless drives based on full-order SMO, in IEEE Transactions on Power Electronics, April 2022; 37(4), 4463–4474, https://doi.org/10.1109/TPEL.2021.3125024
23. Park Y. and Sul S. -K., Sensorless Control Method for PMSM Based on Frequency-Adaptive Disturbance Observer, in IEEE Journal of Emerging and Selected Topics in Power Electronics, June 2014; 2(2), 143–151, https://doi.org/10.1109/JESTPE.2013.2296596
24. Yoon Y. -D., Sul S. -K., Morimoto S. and Ide K., High-bandwidth sensorless algorithm for AC machines based on square-wave-type voltage injection, in IEEE Transactions on Industry Applications, May-June 2011; 47(3), 1361–1370, https://doi.org/10.1109/TIA.2011.2126552
25. Holtz J., Sensorless control of induction machines—with or without signal injection?, in IEEE Transactions on Industrial Electronics, Feb. 2006; 53(1), 7–30, https://doi.org/10.1109/TIE.2005.862324
26. Zhang T., Xu Z. and Gerada C., A nonlinear extended state observer for sensorless IPMSM drives with optimized gains, in IEEE Transactions on Industry Applications, March-April 2020; 56(2), 1485–1494, https://doi.org/10.1109/TIA.2019.2959537
27. Li S. Q., Zhang S. X., Liu Y. N., Zhou S. W. Parameter-tuning in active disturbance rejection controller using time scale. Control Theory & Applications, 2012; 29(1), 125–129.
28. Mubarok M. S. and Liu T. -H., An adjustable wide-range speed-control method for sensorless IPMSM drive systems, in IEEE Access, 2022; 10, 42727–42738, https://doi.org/10.1109/ACCESS.2022.3168390
29. Tarczewski T., Szczepanski R., Erwinski K., Hu X. and Grzesiak L. M., A novel sensitivity analysis to moment of inertia and load variations for PMSM drives, in IEEE Transactions on Power Electronics, Nov. 2022; 37(11), 13299–13309, https://doi.org/10.1109/TPEL.2022.3188404
30. Kuttey V. K., Bali S. K. (2024). Effect of Number of Poles on IPMSM Performance for Electric Vehicle Drivetrain. In: Malik, H., Mishra, S., Sood, Y.R., Iqbal, A., Ustun, T.S. (eds) Renewable Power for Sustainable Growth. ICRP 2023. Lecture Notes in Electrical Engineering, vol 1086. Springer, Singapore. https://doi.org/10.1007/978-981-99-6749-0_47
31. Kuttey V. K. and Bali S. K., Effect of Various Drive Cycles on Battery Electric Vehicle (BEV), 2024 International Conference on Computational Intelligence for Green and Sustainable Technologies (ICCIGST), Vijayawada, India, 2024; 1–4, https://doi.org/10.1109/ICCIGST60741.2024.10717587
32. Awtoniuk M., The application of the model mismatch strategy to improve speed control accuracy of prototype systems, Advances in Science and Technology Research Journal (ASTRJ), 2025.
33. Katkar V. A., Goswami P., Devarapalli R. and Yashwante M. R., Rule-based Hybrid Energy Storage System Design and Control of an Electric Vehicle, 2024 International Conference on IoT, Communication and Automation Technology (ICICAT), Gorakhpur, India, 2024; 902–908, https://doi.org/10.1109/ICICAT62666.2024.10923323
34. Knypiński Ł., Devarapalli R., Gillon, F. The hybrid algorithms in constrained optimization of the permanent magnet motors. IET Science, Measurement & Technology, 2024; 18(9), 455–461.
35. Reddy V., Venkateswararao B., Knypiński Ł. and Devarapalli R., Sizing of the Switched Reluctance Motor for Electric Vehicles, 2023 Progress in Applied Electrical Engineering (PAEE), Koscielisko, Poland, 2023; 1–4, https://doi.org/10.1109/PAEE59932.2023.10244727
36. Romowicz B., Machno M., Weigel-Milleret K. A study on the electric energy consumption of a lightweight four-wheeled vehicle powered by the hub-mounted brushless direct-current hub motors designed for disabled people. Advances in Science and Technology Research Journal, 2025; 19(10), 173–187. https://doi.org/10.12913/22998624/208036